

CAAP Quarterly Report

Date of Report: *January 7, 2020*

Prepared for: *Thomas Finch (Project Manager) and Joshua Arnold (CAAP Program Manager), U.S. DOT Pipeline and Hazardous Materials Safety Administration*

Contract Number: *693JK31850005CAAP*

Project Title: *Low-variance Deep Graph Learning for Predictive Pipeline Assessment with Interacting Threats*

Prepared by: *Hao Zhang (Colorado School of Mines) and Yiming Deng (Michigan State University)*

Contact Information: *Dr. Hao Zhang, Department of Computer Science, Colorado School of Mines; 1500 Illinois St., Golden, CO 80401; Phone: 303-273-3581; Email: h Zhang@mines.edu*

For quarterly period ending: *January 7, 2020*

Business and Activity Section

(a) Contract Activity

No contract modification was made or proposed in this quarterly period. No materials were purchased during this quarterly period.

(b) Status Update of Past Quarter Activities

In this reporting period, the research team performed comprehensive literature review, and made progress toward achieving the technical objectives including:

- (1) Starting the work on the development of CNN-based deep learning for low-variance interacting threats characterization (Task 3.1).
- (2) Completed the work on spatiotemporal interacting threat modeling by graphs (Task 4.1).

In this reporting period, the research team made progress on educational activities, including involving three PhD students and several unpaid master and undergraduate students at Mines and MSU, and adapting the research topics from this project with undergraduate research programs (e.g., the Mines Undergraduate Research Honor Thesis) and MSU (e.g., ENSURE program).

(c) Cost Share Activity

PI Zhang used his 11.29% yearly effort as the in-kind cost share to work on the project at the Colorado School of Mines. Co-PI Yiming Deng used his 6.07% yearly effort as the in-kind cost

share to work on the project at the Michigan State University. The cost share was used following the approved proposal and no modification was made.

1. Progress on Task 3.1: CNN-based deep learning for low-variance interacting threats characterization

1.1. Simulation Environment Specification

The goal of current simulation is to establish the link between multi-NDE sensing measurements and defect profile, which will help us to develop probabilistic models of failure pressure of a pipeline containing defects, achieving predictions that are unbiased with reduced variability. Numerical data (i.e., FE analysis results) in our study should also be well managed as well as specifying simulation environment to be better compared with future experimental results. MFL and PEC probe specifications are listed as follows:

Table 1: MFL simulation specification

Magnetic source specification	Value
MUT is magnetized by permanent magnets such as NdFeB	Select
MUT is magnetized by a ferrite core with a N-turn coils	
Residual magnetism	50000 A/m on z direction
Coercive force	
Lift-off value	3 [mm]
Length of yoke	320 [mm]
Thickness of yoke	30 [mm]
Width of yoke	30 [mm]
Length of brush	30 [mm]
Thickness of brush	20 [mm]
Width of brush	30 [mm]
Length of magnets	30 [mm]
Width of magnets	30 [mm]
Thickness of magnets	20 [mm]

Table 2: PEC simulation specification

Quantity	Value
Thickness of PEC coils	2 [mm]
Length of excitation coil	25 [mm]
Width of excitation coil	25 [mm]
Length of pick-up coils	22 [mm]

Width of pick-up coils	22 [mm]
Lift -off value	3 [mm]
Excitation coil turns	100
Pick -up coil turns	300
Type of core material	Copper
Presence of shield	No
Excitation current density	Supplied by a pulsed voltage source
Duration of rising edge	0.2 [μ s]
Pulse width	2.5 [μ s]
Amplitude of the excitation current/voltage	Voltage of 10[V]
Durations of Falling edge	0.2 [μ s]

Table 3: Data form of PEC results

Densities and distribution patterns of induced eddy currents	In matrix form
Readings from pick-up coil	Vector
Amplitude of the rising peak of differential induced voltage	Scalar
Time-to-peak	Scalar

Table 4: Data form of MFL results

Leakage flux density on x, y, z direction measured by magnetic field sensor	
B_x	In matrix form
B_y	In matrix form
B_z	In matrix form
Differential form (for artificial defect)	
ΔB_x	In matrix form
ΔB_y	In matrix form
ΔB_z	In matrix form

1.2. Simulation Data Management

In this report, design of location arrangement for multi-defect data is illustrated.

The demonstrated approach can be efficiently applied to generating simulated measurements on a larger domain with multiple interacting threats.

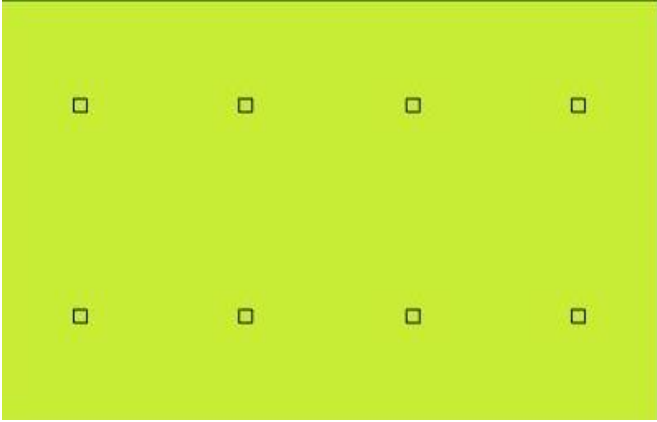


Figure 1: Multiple defect location arrangement

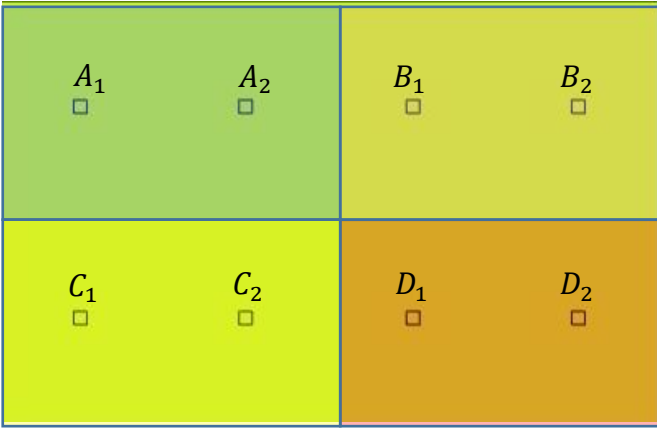


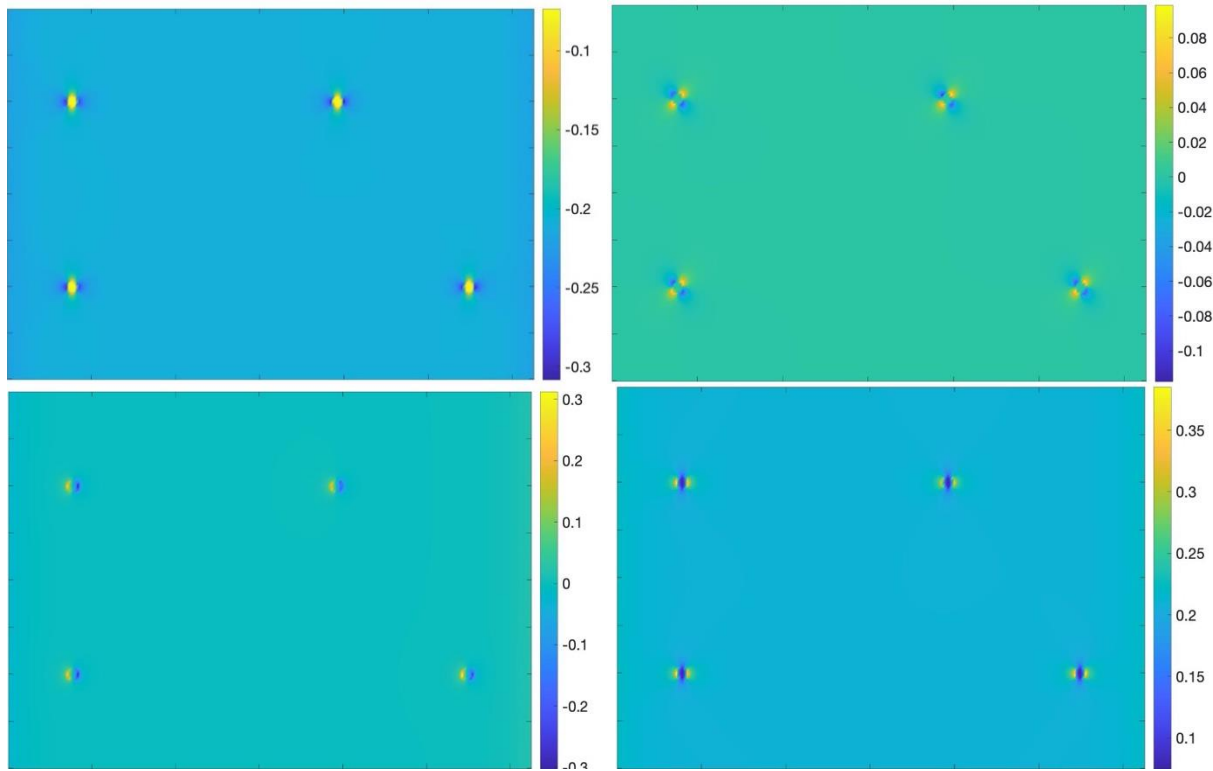
Figure 2: Predefined defects selection scheme based on section A, B, C and D segmentation

Table 5: Location of predefined defects

A_1	(-94.25,40)
A_2	(-31.75,40)
B_1	(31.75,40)
B_2	(94.25,40)
C_1	(-94.25, -40)
C_2	(-31.75, -40)
D_1	(31.75, -40)
D_2	(94.25, -40)

Combination	<i>A</i>	<i>B</i>	<i>C</i>	<i>D</i>
X	1	2	1	1

For instance, when (1,2,1,1) is given $A_1; B_2; C_1; D_1$ are selected as primary defects in the geometric set up, then existing modelling information is incorporated to complete the whole design.



In the end, by drawing one defect from each section, 16 combinations in terms of defects distribution are generated

Combination	<i>A</i>	<i>B</i>	<i>C</i>	<i>D</i>
No.1.	1	1	1	1
No.2.	1	1	1	2
No.3.	1	1	2	1
No.4.	1	1	2	2
No.5.	1	2	1	1
No.6.	1	2	2	2
No.7.	1	2	1	2
No.8.	1	2	2	1
No.9.	2	1	1	1
No.10.	2	1	1	2

No.11.	2	1	2	1
No.12.	2	1	2	2
No.13.	2	2	1	1
No.14.	2	2	2	2
No.15.	2	2	1	2
No.16.	2	2	2	1

1.3. Basic Interacting Threats Study

Stress corrosion cracking (SCC) in pipelines is the cracking of a metal or alloy by the combined action of stress and the environment, SCC is considered as the primary cause of failure, which is simulated and analyzed in MSU's study. There are three criteria must be met for SCC formation

- (1) A threshold stress or stress intensity must be exceeded for SCC to occur;
- (2) The material must be susceptible to SCC;
- (3) Corrosive environments must be present in order to cause SCC in certain alloys [5, 6].

The presence of SCC cracks reduces the cross section of the metal capable of carrying a load. In COMSOL based simulation study we conducted so far, reduced cross section of the sample is independent of supporting structure nearby, which is different from real-life scenario and requires further studies.

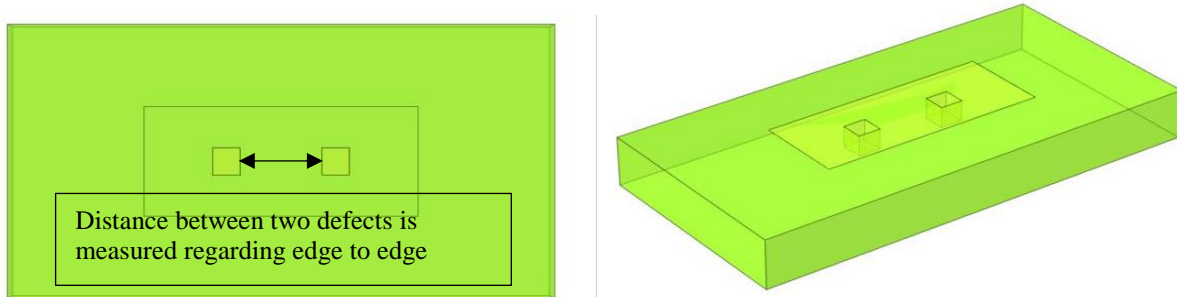


Figure 3: Modelling of interacting threats model under MFL inspection

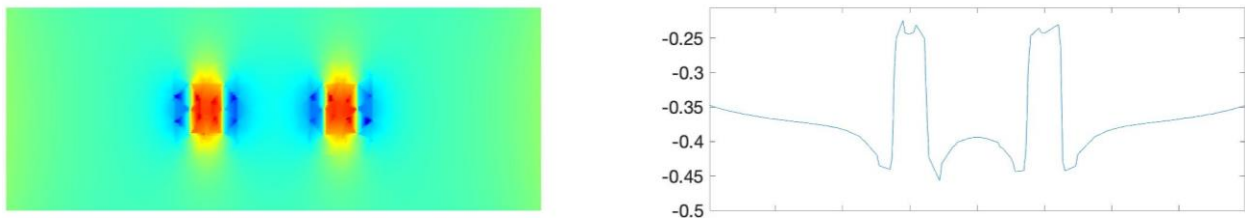


Figure 4: Measurement of Bx on defects of distance 15[4], center line plot is illustrated on the right side

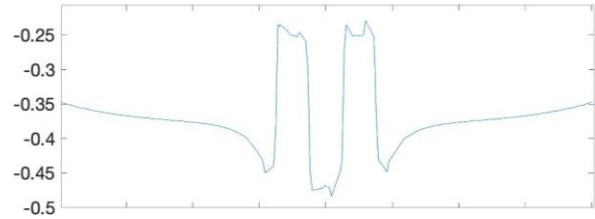
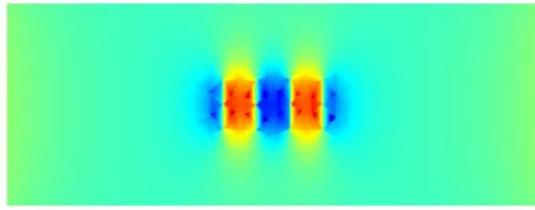


Figure 5: Measurement of Bx on defects of distance 5[4], center line plot is illustrated on the right side

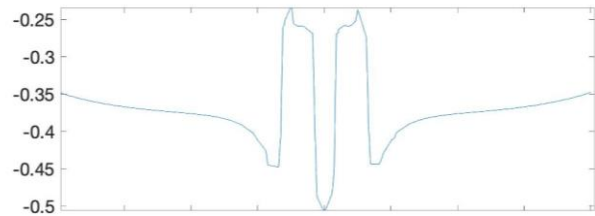
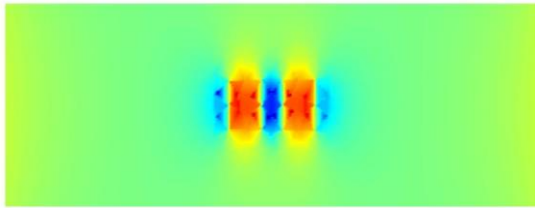


Figure 6: Measurement of Bx on defects of distance 3 [4], center line plot is illustrated on the right side

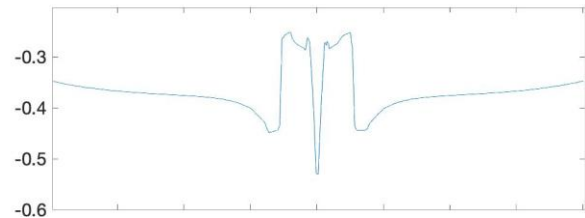
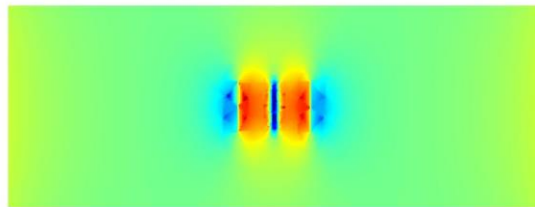


Figure 7: Measurement of Bx on defects of distance 1[4], center line plot is illustrated on the right side

These figures above show the response of MFL inspection on a pair of threats. As we put them closer to each other, the effect of interacting threats could be observed, especially in the center line graph.

References

1. *The "Risk Modeling Work Group" Discussion of Interactive Threats*. 2013.
2. Chen, Y., et al., *Failure assessment of X80 pipeline with interacting corrosion defects*. *Engineering Failure Analysis*, 2015. **47**: p. 67-76.
3. America, I.N.G.A.o., *Interacting Threats to Pipeline Integrity – Defined and Explained*.
4. Guo, J., P. Hu, and J. Tan, *Analysis of a Segmented Annular Coplanar Capacitive Tilt Sensor with Increased Sensitivity*. *Sensors (Basel)*, 2016. **16**(1).
5. McCafferty, E., *Introduction to Corrosion Science*. 2010: Springer.

6. Beauregard, Y. and C. Edwards, *Analysis of severe circumferential SCC found on an ethane pipeline*. The Journal of Pipeline Engineering, 2015: p. 23-32.

2. Progress on Task 4.1: Spatiotemporal interacting threat modeling by graphs

In this quarter, we have evaluated our proposed thread segmentation method and spatiotemporal graph matching method on a simulated pipeline thread dataset.

2.1. Evaluation of the Developed Segmentation Method

In order to evaluate our segmentation method, we first utilize the simulation dataset that contains only single individual simulated threads.

2.1.1. Approach Overview

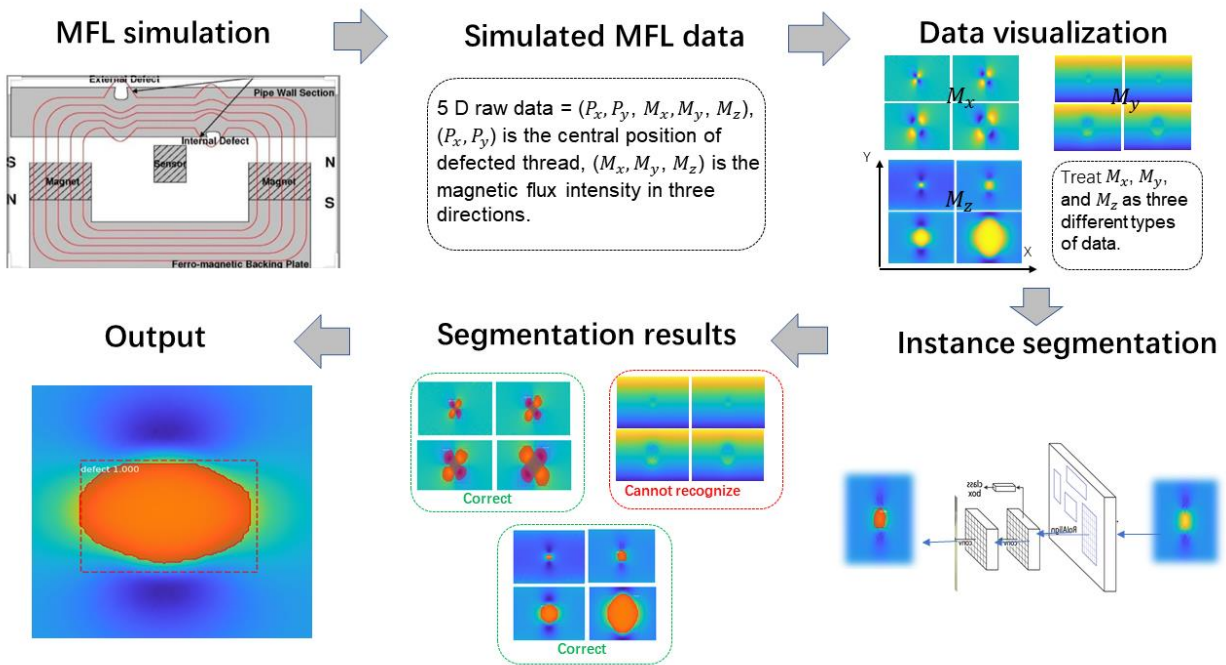


Figure 1 Whole pipeline of our proposed segmentation method

We use the MFL simulation dataset as input, in which each data instance includes 5 kinds of information. The 5D raw data = $(P_x, P_y, M_x, M_y, M_z)$ where (P_x, P_y) is the central position of defected thread, (M_x, M_y, M_z) is the magnetic flux intensity in three directions. The position information is used for the spatiotemporal graph matching and provides the position of threads on pipeline. For the magnetic flux intensity, it is used for the segmentation which can be used to segment threads. In this project, we treat M_x, M_y, M_z as three different types of sensing data,

which is collected from three different direction of MFL. For each type of data, such as M_x , we apply it into our Mask-RCNN segmentation architecture and the output includes three kinds of information including the mask of thread, the type of thread with the corresponding confidence and the boundary of the detected thread. The mask of thread can be used to accurately extract thread visual feature, the thread type with confidence can be used to provide attribute feature of threads and the boundary can be used to provide the central position of threads.

2.1.2. Simulation Datasets

As illustrated in Figure 2, our MFL simulation dataset includes three types of data. Given the visualization of simulation data, we can see that the size of magnetic flux intensity reflects the severity of threads. For a single thread, if we detect it from different direction, then the pattern of the intensity is different. However, for each type of data, all the patterns of thread with different sizes are the same. Thus, we can use our proposed segmentation method to detect the unique pattern in order to segment threads.

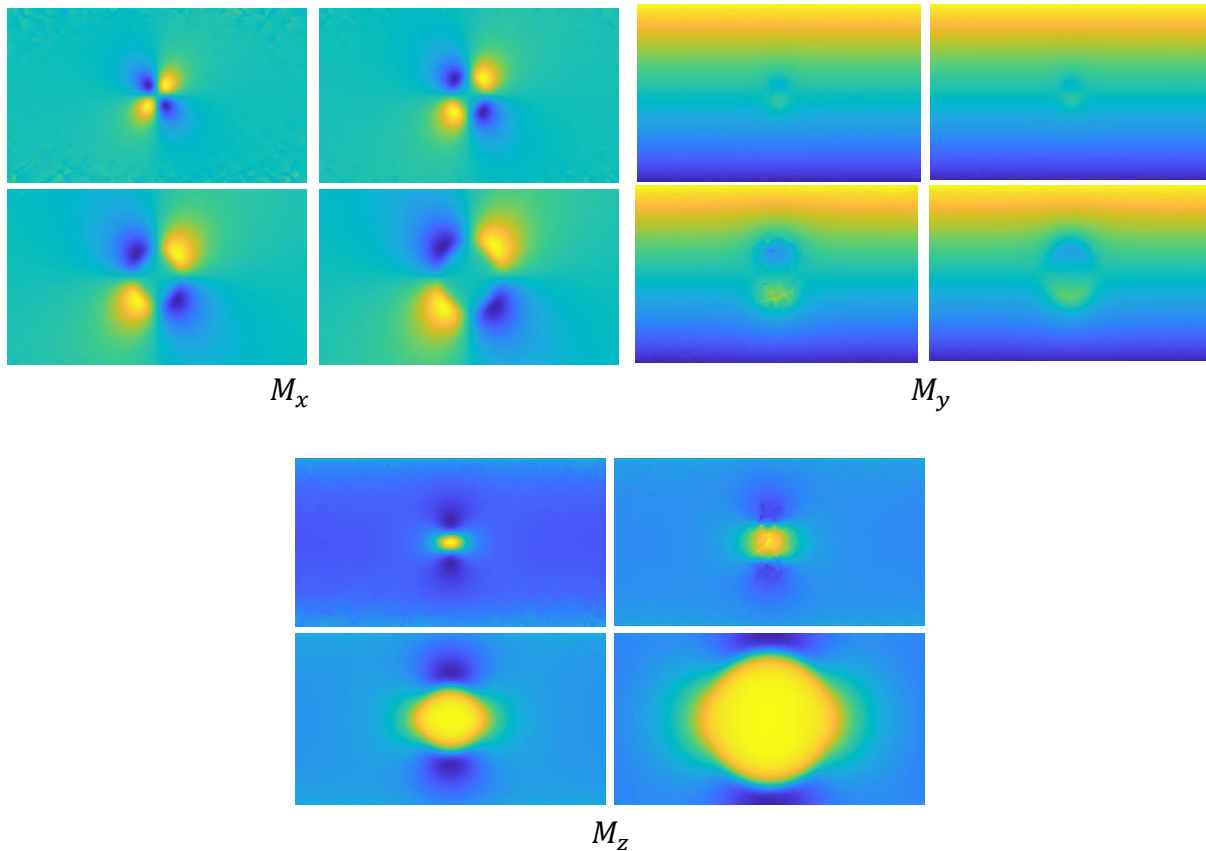


Figure 2 Example of simulation data in three direction

2.1.3. The Developed Segmentation Approach

We use Mask-RCNN architecture to do the segmentation task. Mask-RCNN is basically an extension of Faster-RCNN which is widely used for object detection.

As shown in Figure 3, Mask-RCNN includes two main stages. For stage 1, we first use ResNet 101 to extract features from input images, the feature extraction process includes the encoder process (C2-C5) and decoder process (P5-P2) which are widely used in current CNN-based feature extraction. Given the features, we put them into region proposal network (RPN) which uses a CNN to generate the multiple Region of Interest (RoI) using a lightweight binary classifier. The classifier returns object/no-object scores. The last step in stage 1 is apply the output of RPN to RoI align network which outputs multiple bounding boxes rather than a single definite one and warp them into a fixed dimension. For stage 2, the wrapped features outputted from stage 1 are fed into fully connected layers which output our final results including the type of thread with confidence, bounding boxes and masks of threads.

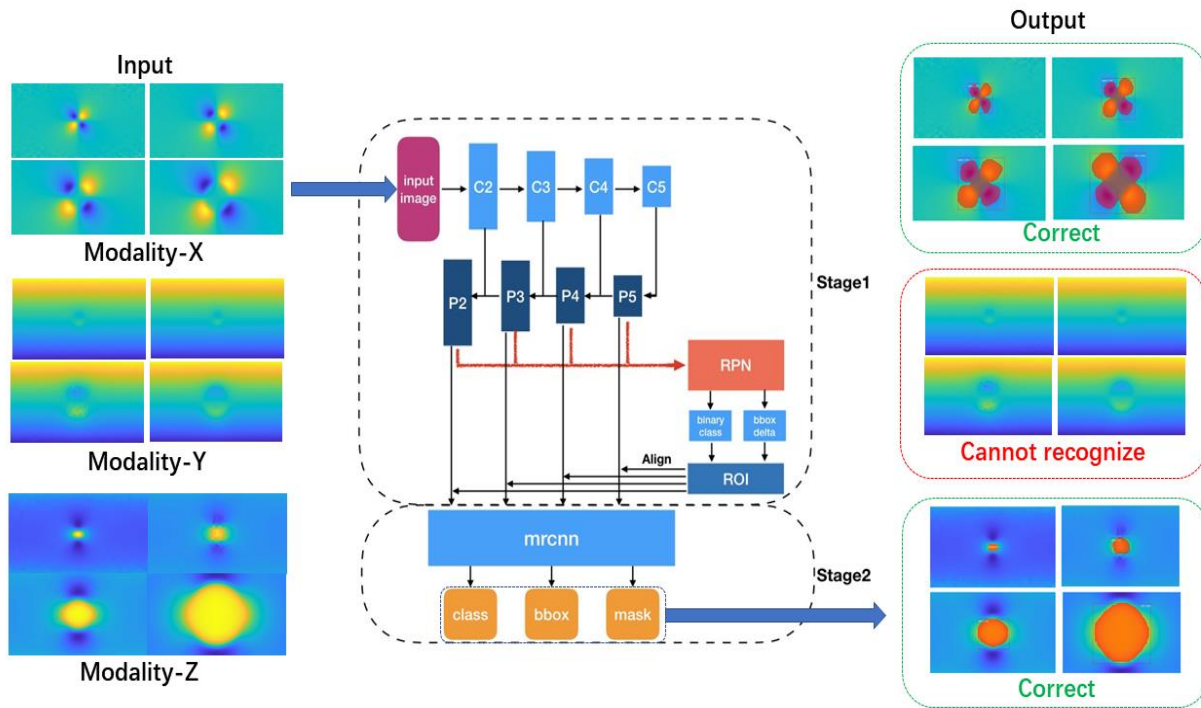


Figure 3 Mask-RCNN for image segmentation

2.1.4. Experimental Analysis

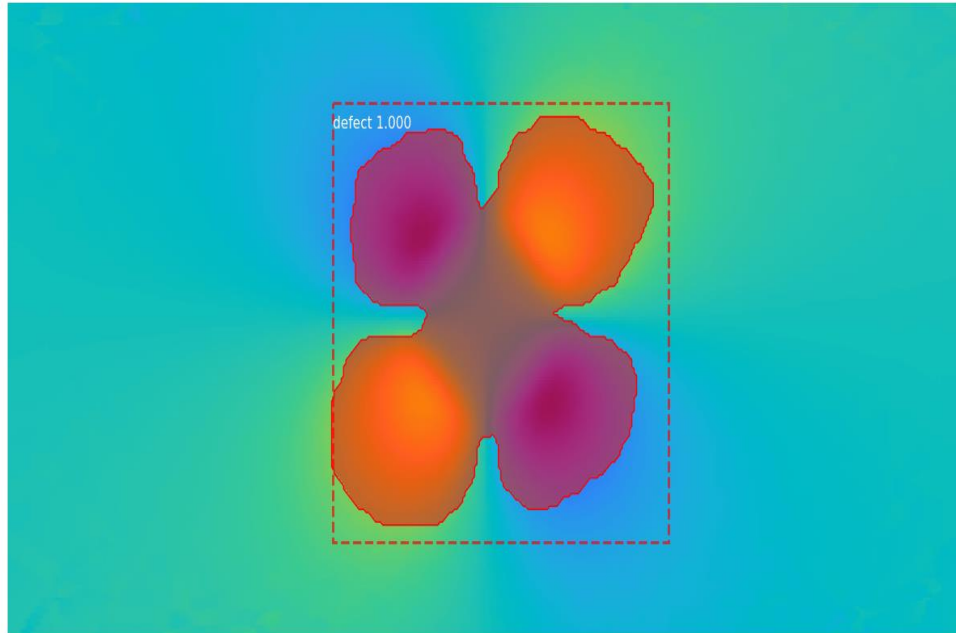


Figure 4-a Segmentation of M_x data type

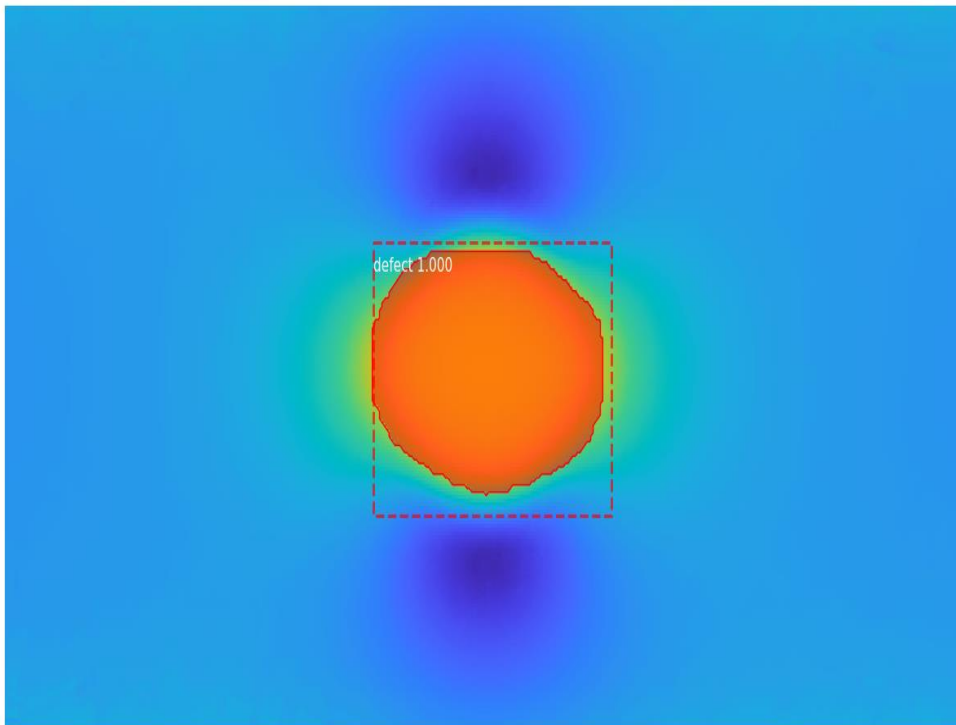


Figure 4-b Segmentation of M_z data type

The final segmentation results are shown in Figure 4. Given the results we can see that the highlight area representing the intensity of magnetic flux is accurately detected. The central position of the bounding box of the thread can be used to localize the position of the thread. Since the thread is very clear and unique in the raw image, the confidence of thread classification is 100%. Since the boundary of the thread in raw image is not clear enough, the mask of the thread can only describe the basic boundary of the thread. We can also see from Figure 3 that M_y data type has very weak intensity of magnetic flux, it is very hard to segment the threads from it. Thus, we only use the other two types of data (M_x, M_z) to segment threads.

2.2. Evaluation of the Developed Spatiotemporal Graph Matching Method

2.2.1. Approach Overview

As shown in Figure 5, we propose a novel visual-spatial information preserving multi-order graph matching method for spatiotemporal matching of threads. The proposed approach takes the region of threads as input, which are localized given our proposed segmentation method. These regions are represented as graph nodes and visual features are extracted from the masks of regions to encode the visual appearances of the nodes. Then, our approach computes distances between two nodes and angles among three nodes to encode the second and third-order spatial relationships, respectively. Thus, the constructed representation integrates both visual and spatial information from an input image. Given graph representations of a pair of query and template images, our approach formulates spatiotemporal matching of threads as a multi-order graph matching problem, which computes a similarity score and node correspondences between the pair of graph representations that encode both visual and spatial cues from the query and template images.

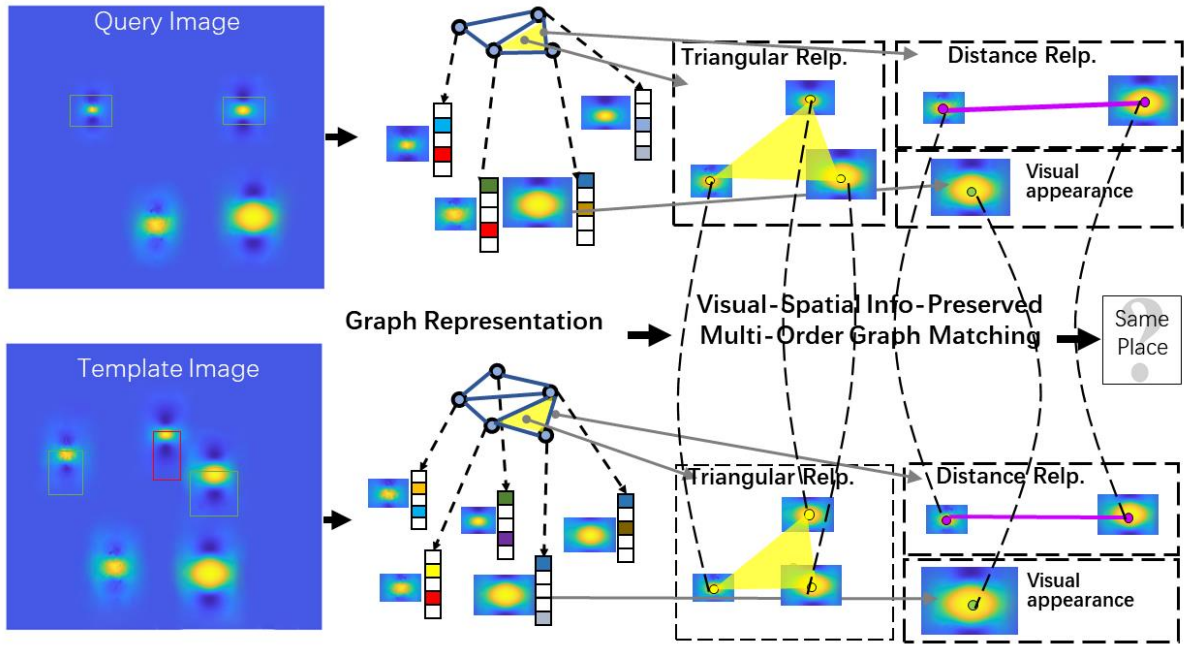


Figure 5 Pipeline of multi-order graph matching method

2.2.2. Simulated Multi-threads Datasets

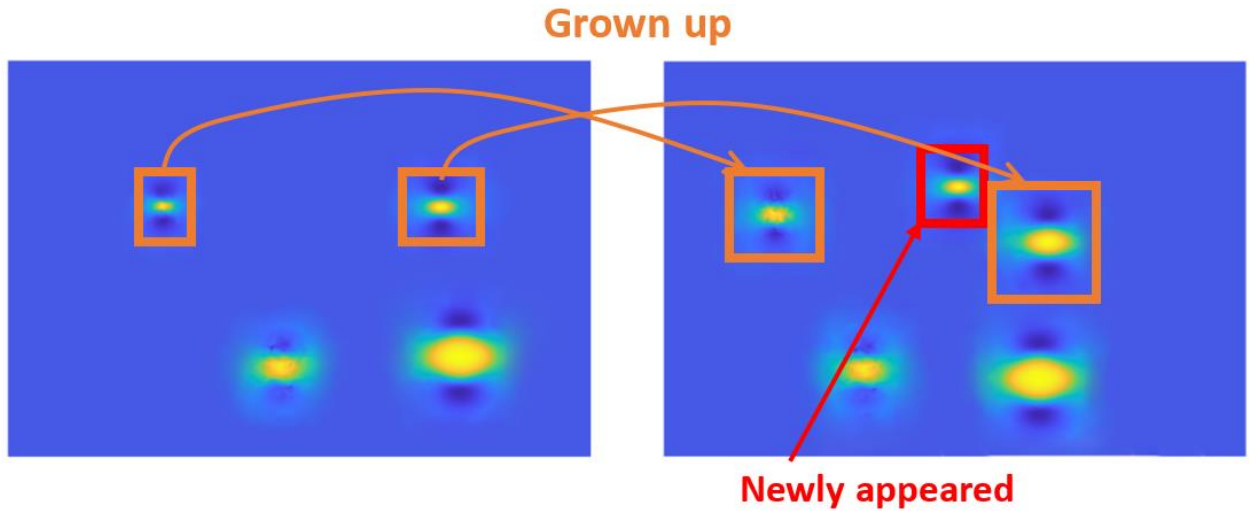


Figure 6 Example of multi-threads data

Besides dataset with single thread, we also mimic the situation with multi-threads in order to evaluate our spatiotemporal graph matching method. Our designed multi-threads dataset is shown as Figure 6, we can see the topology of the threads can represent the spatial information of threads. The right image denotes the evolution of multi-threads from left image (not the real case, we manually generate Figure 6). Given our generated multi-threads data, we can see that

the data describe the evolution of threads, including growing up threads, newly appeared threads.

2.2.3. The Developed Spatiotemporal Graph Matching Approach

In this subtask, we complete the spatiotemporal matching algorithm to identify the corresponding interacting thread appearing in different times. We propose to use graph matching based method to implement this goal. Our designed spatiotemporal graph matching formulation is defined as following:

$$\mathbf{X}^* = \arg \max(\mathbf{T} \otimes \mathbf{X} \otimes \mathbf{X} \otimes \mathbf{X} + \mathbf{X}^T \mathbf{P} \mathbf{X} + \mathbf{B}^T \mathbf{X})$$

The first term is to calculate the angular similarity between two graphs, the second term is used to compute the distance similarity between graphs and the last term is to calculate the similarity of defect appearances (like shape) between two graphs. The matrix \mathbf{X} is the final corresponding matrix which encodes the correspondences of nodes in two graphs. The mathematical detail of this approach has been reported in previous reports.

2.2.4. Experimental Analysis

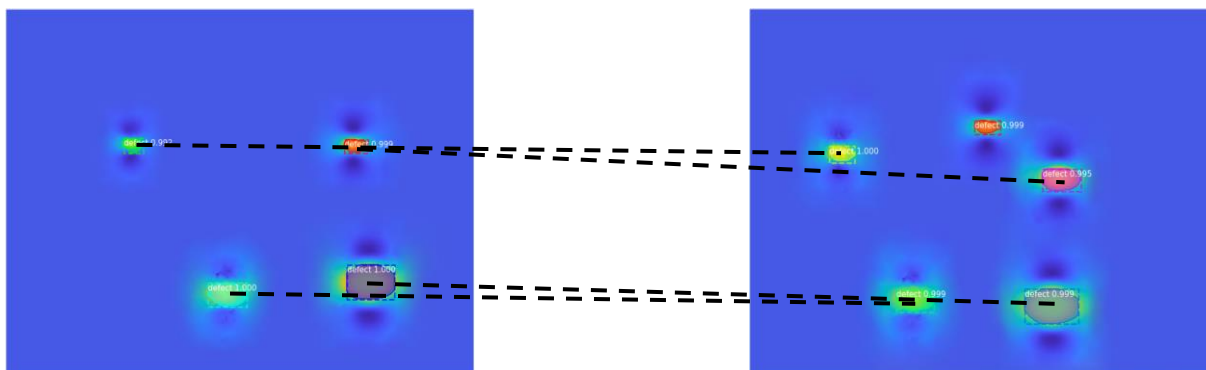


Figure 7 Spatiotemporal graph matching result

As shown in Figure 7, we can see that our proposed spatiotemporal graph matching method can correctly identify the correspondences between two images recorded at different times. The left image in Figure 7 is recorded at inspection 1 and the right image is recorded at inspection 2 (after some time from the first inspection). Even though there exist newly appeared and growing up thread, our proposed method can still find the correct correspondences.

2.3. Summary and Future Work

In this report, we use the simulated pipeline threads dataset to evaluate our proposed image segmentation method and spatiotemporal graph matching method. The quantitative results shown

the effectiveness of our methods. Given the output from image segmentation, we can obtain the visual feature and position of threads and then we use these features to do graph matching in order to identify the spatiotemporal correspondences between different images (inspection) recorded at different times. Given the output of spatiotemporal matching of threads, we will implement the RNN-based prediction model in the next in order to prediction the remaining strength or failure pressure of pipeline.